Control of near-infrared supercontinuum bandwidth by adjusting pump pulse duration

M. Andreana,[1,2] A. Labruyère,[1] A. Tonello,[1] S. Wabnitz,[2] P. Leproux,[1,4] V. Couderc,[1,*] C. Duterte,[3] A. Cserteg,[3] A. Bertrand,[3] Y. Hernandez,[3] D. Giannone,[3] S. Hilaire,[4] and G. Huss[4]

[1]*Université de Limoges, XLIM, UMR CNRS 7252, 123 av. A. Thomas, 87060 Limoges, France*
[2]*Dipartimento di Ingegneria dell'Informazione, Università di Brescia, via Branze 38, 25123 Brescia, Italy*
[3]*Multitel asbl, Parc Initialis, 2 rue Pierre et Marie Curie, 7000 Mons, Belgium*
[4]*Leukos Innovative Optical Systems, Ester Technopole, 1 av. d'Ester, 87069 Limoges, France*
[*]*vincent.couderc@xlim.fr*

Abstract: We experimentally and numerically investigated the impact of input pump pulse duration on the near-infrared bandwidth of supercontinuum generation in a photonic crystal fiber. We continuously stretched the temporal duration of the input pump laser (centered at 1030 nm) pulses from 500 fs up to 10 ps, while keeping fixed the pump peak power. We observed that the long-wavelength edge of the supercontinuum spectrum is increased by 200 nm as the pump pulse duration grows from 500 fs to 10 ps. We provide a quantitative fit of the experimental results by means of numerical simulations. Moreover, we have explained the observed spectral broadening enhancement induced by pump pulse energy by developing an approximate yet fully analytical model for soliton energy exchange through a series of collisions in the presence of stimulated Raman scattering.

OCIS codes: (190.4370) Nonlinear optics, fibers; (060.5530) Pulse propagation and temporal solitons.

References and links

1. J. M. Dudley, G. Genty, and S. Coen, "Supercontinuum generation in photonic crystal fiber," Rev. Mod. Phys. **78**, 1135–1184 (2006).
2. J. K. Ranka, R. S. Windeler, and A. J. Stentz, "Visible continuum generation in air-silica microstructure optical fibers with anomalous dispersion at 800 nm," Opt. Lett. **25**, 25–27 (2000).
3. S. Coen, A. H. L. Chau, R. Leonhardt, J. D. Harvey, J. C. Knight, W. J. Wadsworth, and P. St. J. Russell, "White-light supercontinuum generation with 60-ps pump pulses in a photonic crystal fiber," Opt. Lett. **26**, 1356–1358 (2001).
4. E. Räikkönen, G. Genty, O. Kimmelma, M. Kaivola, K. P. Hansen, and S. C. Buchter, "Supercontinuum generation by nanosecond dual-wavelength pumping in microstructured optical fibers," Opt. Express **14**, 7914–7923 (2006).
5. A. Mussot and A. Kudlinski, "19.5 W CW-pumped supercontinuum source from 0.65 to 1.38 μm," Electron. Lett. **45**, 29–30 (2009).
6. E. E. Serebryannikov and A. M. Zheltikov, "Supercontinuum generation through cascaded four-wave mixing in photonic-crystal fibers: when picoseconds do it better," Opt. Commun. **274**, 433-440 (2007).
7. A. Mussot, M. Beaugeois, M. Bouazaoui, and Th. Sylvestre, "Tailoring CW supercontinuum generation in microstructured fibers with two-zero dispersion wavelengths," Opt. Express. **15**, 11553–11563 (2007).
8. M. Erkintalo, G. Genty, and J. M. Dudley, "On the statistical interpretation of optical rogue waves," Eur. Phys. J. Special Topics **185**, 135–144 (2010).

#159739 - $15.00 USD Received 12 Dec 2011; revised 9 Feb 2012; accepted 27 Feb 2012; published 25 Apr 2012

9. M. N. Islam, G. Sucha, I. Bar-Joseph, M. Wegener, J. P. Gordon, and D. S. Chemla, "'Femtosecond distributed soliton spectrum in fibers," J. Opt. Soc. Am. B **6**, 1149–1158 (1989).
10. M. H. Frosz, O. Bang, and A. Bjarklev, "Soliton collision and Raman gain regimes in continuous-wave pumped supercontinuum generation," Opt. Express **14**, 9391–9407 (2006).
11. F. Luan, D. V. Skryabin, A. V. Yulin, and J. C. Knight, "Energy exchange between colliding solitons in photonic crystal fibers," Opt. Express **14**, 9844–9853 (2006).
12. Q. M. Nguyen and A. Peleg, "Resolving the Raman-induced cross frequency shift in fast optical soliton collisions," J. Opt. Soc. Am. B **27**, 1985–1990 (2010).
13. S. Kumar, "Influence of Raman effects in wavelength-division multiplexed soliton systems," Opt. Lett. **23**, 1450–1452 (1998).
14. J. P. Gordon, "Theory of the soliton self-frequency shift," Opt. Lett. **11**, 662–664 (1986).
15. J. Herrmann and A. Nazarkin, "Soliton self-frequency shift for pulses with a duration less than the period of molecular oscillations," Opt. Lett. **19**, 2065–2067 (1994).
16. A. C. Judge, O. Bang, B. J. Eggleton, B. T. Kuhlmey, E. C. Mägi, R. Pant, and C. Martijn de Sterke, "Optimization of the soliton self-frequency shift in a tapered photonic crystal fiber," J. Opt. Soc. Am. B **26**, 2064–2071 (2009).
17. N. N. Akhmediev, V. M. Eleonskii, and N. E. Kulagin, "Generation of periodic trains of picosecond pulses in an optical fiber: Exact solutions," Sov. Phys. JETP **62**, 894–992 (1985).
18. N. N. Akhmediev and V. I. Korneev, "Modulation instability and periodic solutions of nonlinear Schrödinger equation," Teor. Mat. Fiz. **69**, 189–194 (1986).
19. J. C. Travers, "Blue extension of optical fibre supercontinuum generation," J. Opt. **12**, 113001 (2011).

1. Introduction

Optical supercontinuum (SC) generation is the nonlinear phenomenon whereby the spectrum of an intense pump beam, either pulsed or continuous wave (CW), is dramatically widened into a palette of wavelengths upon propagation in a nonlinear dispersive medium such as an optical fiber. Among recent applications of SC sources, we may list laser-frequency metrology and biomedical imaging [1]: both technologies take advantage of the high spectral brightness of these sources. Since the early demonstrations of optical SC generation, it has been clear that the pump pulse duration plays a key role in determining the mechanism of nonlinear spectral broadening [1, 2]. As a matter of fact, many in-depth studies of SC generation with pump durations ranging from sub-picosecond to nanosecond and even CW excitation have been separately performed. When using relatively short pump pulses, one obtains high peak power and high repetition rate SC sources. Whereas nanoseconds and CW pump lasers enable low-cost and compact solutions for SC sources [3–5]. A suitable combination of the pump pulse duration and group-velocity dispersion permits to select a specific nonlinear mechanism for activating frequency generation and spectral broadening in optical fibers (see, e.g. [6]). With sub-ps pump pulses, even in the early stages of propagation one obtains multiple soliton fission and soliton self-frequency shift (SSFS) owing to Raman scattering. Whereas for relatively long (i.e., ns or sub-ns) pulses or CW, SC generation is first initiated by modulational instability (MI), followed by the formation and fission of a periodic soliton train [7].

In this work we have carried out a systematic experimental and theoretical study of the dependence of the SC spectral broadening upon the continuous variation of the pump pulse temporal duration. Moreover, we have studied, by means of a fully analytical method, the underlying physical mechanism that governs such spectral broadening in optical fibers. In our experiment, we have used a femtosecond laser at 1030 nm and a chirped pulse amplification scheme which permitted us to vary the input pulse duration between 500 fs up and 10 ps. At the same time, the peak power was fixed at the constant value of 3 kW. We have continuously monitored the laser power by using a fiber coupler: the optical power was measured at one output arm, while the other arm was spliced with the PCF. By varying the input pulse duration with a fixed peak power, we could continuously change both the pump pulse energy and the number of MI-generated solitons that are injected in the fiber by 20 times, while keeping the individual soliton parameters (*i.e.* peak power and time duration) unchanged. The 20-fold increase of the pump pulse duration (or energy) leads to about 200 nm of enhancement of the SC bandwidth in

#159739 - $15.00 USD Received 12 Dec 2011; revised 9 Feb 2012; accepted 27 Feb 2012; published 25 Apr 2012

the short-wave infrared (*i.e.* from 1200 up to 1400 nm). Such pump-pulse energy enhancement of the spectral broadening was confirmed by numerical simulations based on the generalized Nonlinear Schrödinger equation (GNLSE):

$$\frac{\partial A}{\partial z}+\frac{\alpha}{2}A-\sum_{n\geq 2}\frac{i^{n+1}}{n!}\beta_n\frac{\partial^n A}{\partial t^n}=i\gamma\left(1+i\tau_S\frac{\partial}{\partial t}\right)\times\left(A(z,t)\int_{-\infty}^{+\infty}\mathscr{R}(t')|A(z,t-t')|^2dt'\right) \quad (1)$$

where α accounts for linear power attenuation, β_n are the dispersion coefficients, γ is the nonlinear coefficient of the fiber at the carrier wavelength, τ_S the self-steepening coefficient and $\mathscr{R}(t)$ accounts for the instantaneous electronic and vibrational (Raman) response of the fiber. The physical mechanism that leads to the observed enhanced spectral broadening on the long-wavelength side of the SC spectrum is the Raman activated energy exchange among solitons of different wavelengths upon their collisions [8]. Because of Soliton Self-Frequency Shift (SSFS), such energy exchange leads to the preferential amplification of the highest peak power soliton that is formed near the peak of the pump pulse. Although this basic principle has been known for a long time [9], in order to obtain a good quantitative agreement between theory and experiments for pump durations ranging from the 100 fs up to the ps timescale it has been necessary to develop a novel and more accurate, yet fully analytical model for the soliton power exchange at collisions.

2. Experimental results

Let us first describe our experimental study of the input pump pulse duration (or energy) dependence of the SC spectral broadening. As a nonlinear medium for SC generation, we employed a sample of 8 m long photonic crystal fiber (PCF) with 5μm core diameter, 3μm hole-to-hole pitch and 0.5 air filling fraction. The full wavelength dependence of the PCF dispersion is obtained by using a standard mode solver and an image of the fiber's cross-section taken from a scanning electron microscope. The PCF zero dispersion wavelength (ZDW) is estimated at 974 nm. In order to control the pump pulse temporal duration, we proceed as follows: we start from a commercial femtosecond oscillator (Amplitude Systèmes) centered at 1030 nm with 30 MHz repetition rate. Its output pulses were temporally stretched by a dispersive element up to 300 ps. At the same time, the pulse repetition rate was reduced to the range of 1 kHz to 300 kHz by a pulse picker based on a Pockels cell. Finally, we obtained pump pulses with adjustable temporal duration between 500 fs to 10 ps by means of an adjustable grating compressor.

On the left-hand side of Fig. 1 we show the experimental output SC spectra for different input pulse durations and under the same input peak power. We monitored the optical power at one port of a fiber coupler, being the PCF spliced to the other port. The available laser peak power was of 3kW; we estimate that splice and coupling loss are of 5-6dB. The two dashed vertical lines indicate the ZDW and the laser carrier wavelength. As it can be seen, on the short-wave infrared side (i.e., between 1μm and 2μm) the spectral broadening is extended by about 200 nm when varying the pump pulse duration from 500 fs up to 10 ps. On the right hand side of Fig. 1 we show the corresponding numerically calculated SC spectra from the full numerical solution of the GNLSE. Numerical spectra were obtained by averaging the calculation results with nine different input noise seeds (one photon per mode model). In all cases, the input peak power was kept fixed as the pulse duration was increased. We assumed a value of 350 W for the input peak power in numerical simulations and 8 m of propagation, and an effective core area varying between 4.68μm^2 (at 1030nm) and 5.7μm^2 (at 1600 nm).

Figure 1 shows that a good agreement between experiments and numerical simulations is obtained at that power value under the different pulse durations. Although the input pulses

#159739 - $15.00 USD Received 12 Dec 2011; revised 9 Feb 2012; accepted 27 Feb 2012; published 25 Apr 2012

from our pump laser were not chirp-free, still a good fit could be obtained with the numerical simulations assuming transform-limited gaussian pulses for simplicity.

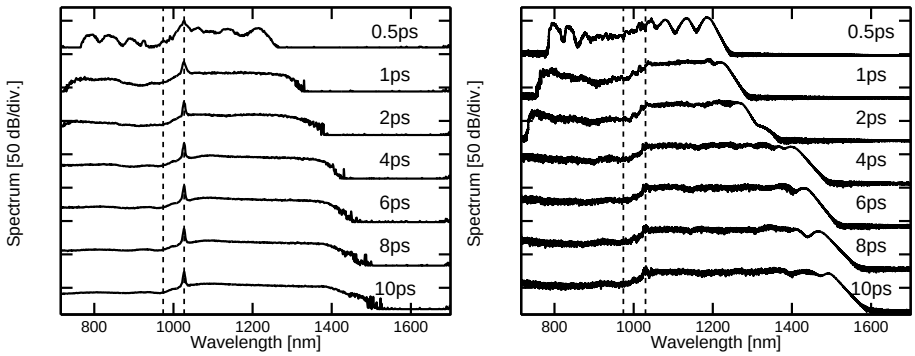

Fig. 1. Left. Experimental output SC spectra for different input pulse durations and constant input peak power of 3 kW. Right. Numerical simulation of the SC spectra, averaged over nine noise seeds. The dashed lines represent the ZDW and the laser central wavelength respectively.

3. Model for soliton collisions

In this section we derive an accurate and fully analytical method to evaluate the Raman-induced energy exchange among solitons which is responsible for the observed increase of the long-wavelength side of the SC spectrum as the pump pulse duration (or energy) grows larger. The colliding solitons are created by MI of the pump pulse propagating in the anomalous dispersion regime of the fiber. It is known that MI breaks up the pump pulse into a train of solitons, whose temporal period is given by the reciprocal of the modulation frequency. Note that the peak intensity of each soliton varies according to their position along the pump pulse profile. As a consequence, adjacent solitons in the train undergo different frequency-down shifts owing to SSFS. Since the SSFS is proportional to the inverse of the soliton duration to the fourth, a soliton which is created in the central part of the input pump pulse down-shifts in frequency (hence decelerates in time owing to dispersion) much faster than its neighboring solitons. The creation of individual first-order solitons is clearly shown by the numerical simulations for the evolution of the pump intensity along the fiber. As first pointed out by Islam et al. [9], when two different frequency solitons collide Raman scattering leads to an energy increase (decrease) for the longer (shorter) wavelength soliton. After multiple collisions, this process leads to a progressive energy enhancement of the most red-shifted soliton. A key hypothesis here, which is confirmed by the numerics, is that the solitons retain their particle nature after each collision. In other words, each soliton is adiabatically reshaped during its propagation in-between any two consecutive collisions, so that its peak power and temporal duration are adjusted to the energy gain (loss) induced by the collision [10]. As a result of all their collisions, each soliton of the train undergoes different SSFS so that a broad SC is generated to the long wavelength side of the pump. In order to provide more physical insight into this process beyond what can be achieved by full-scale GNLSE simulations, it proves convenient both from a fundamental and a computational point of view to formulate a simplified analytical model that is still able to describe the trajectory of each individual soliton of the train (like in a cloud chamber for experiments in high energy physics). As a matter of fact, it is clear that a proper understanding of the soliton energy enhancement that results from multiple collision is important for correctly predicting the large soliton frequency down-shifts that are observed in the process of SC gener-

#159739 - $15.00 USD Received 12 Dec 2011; revised 9 Feb 2012; accepted 27 Feb 2012; published 25 Apr 2012

ation in optical fibers [10]. A more complete model for collision of a few femtosecond solitons can be found in Ref. [11]

To this end, it is necessary to adapt and refine the model of Ref. [9] so that it can be properly applied to describe our SC generation experiments. First of all it is necessary to include in the model the finite bandwidth of Raman gain, since in some cases the Raman amplified soliton time duration may approach the molecular oscillation period, which for silica glass is $T_m \simeq 75$fs. In addition, two colliding solitons may reach frequency separations which are comparable to or even larger than the Raman gain bandwidth. Both conditions conspire to degrade the energy transfer efficiency with respect to the simple model of Ref. [9]. Next it is necessary to go beyond the undepleted pump approximation when describing the Raman induced energy exchange process among solitons. In other words, a proper book-keeping of the energy of each soliton in the train must be maintained through the entire process. Otherwise one would predict a fixed power gain per collision [9]: when the number of collisions is important, this would strongly overestimate the overall SSFS (hence the SC bandwidth). Clearly our soliton interaction model is based on the assumption that the various disturbances to soliton propagation are of pertubative nature. This permits us to neglect higher order effects such as dispersive wave generation, multiple rather than simply pairwise collisions, and any other possible non adiabatic distortions of the soliton phase and amplitude profile.

Let us proceed by explaining the details of our modifications to the analysis of Ref. [9] in order to fit our experimental situation. We call $u_1(t)$ and $u_2(t)$ the two interacting first-order solitons separated by the frequency detuning Ω. For sake of clarity, we may suppose that $u_2(t)$ is the pump and $u_1(t)$ is the Stokes soliton, respectively. To evaluate the energy exchange per collision we will neglect the frequency dependence of the nonlinear coefficient. In what follows we will also neglect the effect of Raman-induced cross-frequency shift [12, 13]. Clearly, in the absence of perturbations, the two solitons would cross each other upon collision with no net change in their frequency or energy. On the other hand, whenever Raman scattering is included as a perturbation, one obtains for $|u_1|^2$ (a similar expression holds for $|u_2|^2$):

$$\frac{\partial |u_1|^2}{\partial z} \simeq -Im\left\{2u_1^* u_2 \int_{-\infty}^{+\infty} f(s) u_1(t-s) u_2(t-s)^* \exp(-i\Omega s) ds\right\} \tag{2}$$

Consider first the limiting situation where the soliton temporal duration is much longer than the molecular oscillation period T_m [9]. In this case we may simplify the integral of Eq. (2) by assuming that the two field envelopes u_1 and u_2 are constant with respect to the integration variable s. When doing so, the integral is simply proportional to the Fourier transform of $F(\Omega) = \mathscr{F}[f(s)]$. For small frequency detuning, one may further approximate $Im[F(\Omega)] \simeq -\Omega t_d$, where $t_d = T_d/\tau_c$ is the Raman gain slope ($T_d \simeq 6fs$ in Ref. [19] and τ_c is the soliton duration). By supposing a weak collision-induced energy exchange, one obtains that the peak power $|u_1|^2$ of the Stokes soliton is enhanced by the factor $G = \exp(4t_d)$ ($|u_2|^2$ is reduced by the same factor G). Note that, under these assumptions, the power enhancement factor does not depend upon the soliton-soliton detuning Ω, since the larger Raman gain which is experienced by larger values of Ω is exactly balanced by the increased temporal walk-off that leads to a faster (hence less effective) collision. Let us consider now the more general situation where the above mentioned restrictions to both the colliding soliton pair pulse durations and relative frequency spacing are removed. We introduce the complex projection coefficient C as:

$$C\int_{-\infty}^{+\infty} |u_1(t)|^2 |u_2(t)|^2 dt = \int_{-\infty}^{+\infty} u_1(t)^* u_2(t) \left[\int_{-\infty}^{+\infty} f(s) u_1(t-s) u_2(t-s)^* \exp(-i\Omega s) ds\right] dt \tag{3}$$

Let us further approximate the s integral in the right hand side of Eq. (2) by its projection on

#159739 - $15.00 USD Received 12 Dec 2011; revised 9 Feb 2012; accepted 27 Feb 2012; published 25 Apr 2012

the function $u_1(t)u_2(t)^*$. By defining the real valued coefficient $Q = -Im[C]$, we may rewrite the system of soliton-soliton coupled power equations in a more compact form as:

$$\frac{\partial |u_1|^2}{\partial z} = 2Q|u_1|^2|u_2|^2, \qquad \frac{\partial |u_2|^2}{\partial z} = -2Q|u_1|^2|u_2|^2 \tag{4}$$

Note that if $u_1(t)$ and $u_2(t)$ are long with respect to T_m, for small values of Ω, Q reduces to Ωt_d as in Ref. [9]. We remind that these equations have been obtained under the hypothesis that the fiber nonlinear coefficient and hence the fiber nonlinear length is constant upon wavelength. In order to solve Eqs. (4) analytically, we fit the soliton pulse with a gaussian *ansatz* , namely we set $|u_1(t)|^2 = P_1(z)exp[-(t^2/a_1^2)]$ and $|u_2(t)|^2 = P_2(z)exp[-(t-\Omega z)^2/a_2^2]$. The fitting coefficients a_1 and a_2 are chosen so that the approximating gaussian pulses have the same peak power $P_{1,2}$ and energy $E_{1,2} = 2\tau_{1,2}P_{1,2}$ of their corresponding exact soliton solutions $|u_1(t)|^2 = P_1(z)Sech^2(t/\tau_1)$ and $|u_2(t)|^2 = P_2(z)Sech^2((t-\Omega z)/\tau_2)$. This hypothesis leads to $a_1 = 2\tau_1/\sqrt{\pi}$ and $a_2 = 2\tau_2/\sqrt{\pi}$. Under these approximations, and for phases of the envelopes independent of time, the complex coefficient C is fixed at each collision. The expression of C in terms of the two interacting pulses reads as:

$$C = \int_{-\infty}^{+\infty} f(s)exp\left[-\frac{s^2}{4}\left(\frac{1}{a_1^2}+\frac{1}{a_2^2}\right)\right] exp(-i\Omega s)ds \tag{5}$$

which is unchanged during the collision since we suppose that collisions only lead to a peak power (or energy) exchange, whereas the durations of the colliding pulses are unchanged. By first inserting the gaussian pulse ansatz in Eq. (4) and then integrating the equations over time t, we obtain the coupled power equations:

$$\begin{cases} \dfrac{dP_1}{dz} = 2QP_1P_2\dfrac{a_2}{\sqrt{a_1^2+a_2^2}}\exp\left(-\dfrac{\Omega^2 z^2}{a_1^2+a_2^2}\right) \\ \dfrac{dP_2}{dz} = -2QP_1P_2\dfrac{a_1}{\sqrt{a_1^2+a_2^2}}\exp\left(-\dfrac{\Omega^2 z^2}{a_1^2+a_2^2}\right) \end{cases} \tag{6}$$

Note in Eqs. (6) that the power coupling coefficient between the two solitons is a gaussian function of distance z (the point $z = 0$ represents the center of their collision), of their frequency detuning Ω and the inverse of their time durations. Moreover Eqs. (6) have the conserved quantity $E = P_1(z)a_1 + P_2(z)a_2$. Indeed, Eqs. (6) have a closed-form solution for any z: thus if we match its asymptotic solution at $z = -\infty$ with the parameters of the two pulses before the collision, then we obtain the pulse parameters after the collision by evaluating its solution at $z = +\infty$. This means that Eqs. (6) may be reduced to a map that provides the output soliton powers after the collision $P_{1,OUT}, P_{2,OUT}$ from the powers before the collision $P_{1,IN}, P_{2,IN}$, namely:

$$P_{1,OUT} = \frac{C_1 a_2 e^{\psi}}{\kappa + a_1 e^{\psi}}, \qquad P_{2,OUT} = C_1 - \frac{C_1 a_1 e^{\psi}}{\kappa + a_1 e^{\psi}} \tag{7}$$

where $\psi = a_2\sqrt{\pi}QC_1/\Omega$, $C_1 = P_{2,IN} + P_{1,IN}a_1/a_2$ and $\kappa = C_1 a_2 e^{-\psi}/P_{1,IN} - a_1 e^{-\psi}$. Note that the limiting case of long pulses (so that $Q \simeq \Omega t_d$) and a weak signal $P_{1,IN} << P_{2,IN}$ the input-output power gain for the Stokes soliton $G = P_{1,OUT}/P_{1,IN} \simeq exp(4t_d)$. Although the derivation of the solution of Eq. (7) requires some approximations, its result is most valuable since it provides the result of each pair-wise collision in closed form. In physical units we considered the nonlinear coefficient at the frequency of the Stokes soliton in order to account for the variation of the nonlinear response of the fiber upon wavelength.

#159739 - $15.00 USD Received 12 Dec 2011; revised 9 Feb 2012; accepted 27 Feb 2012; published 25 Apr 2012

In order to verify the accuracy of our analytical approach, we compared on the left panel of Fig. 2 the predictions of Eqs. (7) (blue curve) with the pair-wise collision power gain for the Stokes soliton that is obtained from either the long pulse expression $G = exp(4t_d)$ (red curve) or the full numerical solution of the GNLSE (green curve), for a wide range of colliding soliton temporal durations between 10 fs and 600 fs. In all cases, the temporal durations of both colliding solitons are the same. For this specific test we have assumed a constant value of group velocity dispersion with wavelength. On the other hand, as the solitons temporal widths are reduced we progressively increased their initial frequency separation in order to avoid the spectral overlap among them. As it can be seen in Fig. 2, both Eqs. (7) and the GNLSE solutions agree quite well in predicting a departure from the simple exponential increase of gain with the inverse of pulse width whenever the soliton duration decreases below T_m. Indeed, for pulse durations below 40 fs the power gain drops as the pulse width is reduced. Although the analytical model overestimates (with respect to the direct GNLSE numerical integration) the power gain factor by a factor ~ 2 for pulse durations below 20 fs, still it is able to correctly capture the physical mechanism behind the relative gain decrease for collisions among ultrashort pulses.

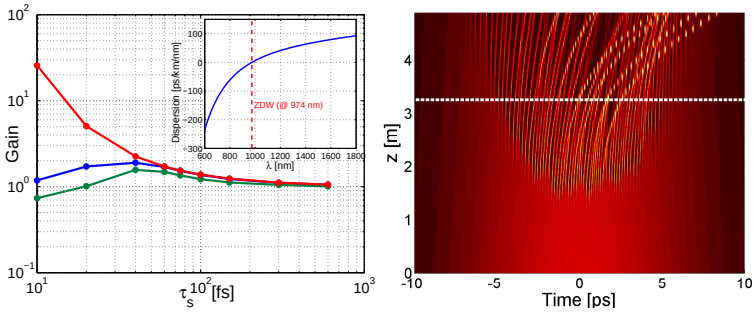

Fig. 2. Left. Red curve: Analytic prediction of gain enhancement valid for long pulses. Blue curve: our analytic prediction of Eqs. (7). Green curve: full numerical solution of the GNLSE. Group velocity dispersion is kept constant for the whole spectral bandwidth for simplicity. Inset: dispersion curve of the PCF used in the experiments and in all other numerical simulations. Right. 10 ps pump pulse break-up and soliton train formation from numerical solution of the GNLSE.

The right panel of Fig. 2 was obtained by the numerical solution of the GNLSE, and illustrates the MI induced break-up of a 10 ps pump pulse into a periodic train of solitons, followed by SSFS and mutual collisions. The dispersion curve is shown in the inset of the left hand panel of the same figure. As it can be seen from the figure, indeed solitons retain their particle-like identity after each collision. Therefore we may conjecture that one may express the near-infrared edge of the SC after the ZDW in terms of a bunch of interacting first order solitons. Then each soliton may be fully characterized in terms of the adiabatic evolution (in between any two collisions) of its parameters, namely its peak power, time duration, central frequency and temporal position. Next, Eq. (7) permits us to compute their mutual power or energy exchange at each pair-wise collision: the Stokes soliton gains energy at the expense of the pump soliton, whereas their time duration remains unchanged during the collision. Moreover, we suppose that each pulse is quickly adiabatically reshaped upon free propagation in the fiber so that both its peak power and time duration are adapted to its new energy after the collision. Namely, we set $\tau_1 = 2\beta_2/\gamma E_{1,OUT}$, $\tau_2 = 2\beta_2/\gamma E_{2,OUT}$, $P_1 = E_{1,OUT}/2\tau_1$, and $P_2 = E_{2,OUT}/2\tau_2$, where β_2 and γ are the group-velocity dispersion and the nonlinear fiber coefficient, respectively. We considered the frequency dependence of β_2 and γ.

We further assume that soliton propagation in-between any two pair-wise collisions is only

#159739 - $15.00 USD Received 12 Dec 2011; revised 9 Feb 2012; accepted 27 Feb 2012; published 25 Apr 2012

affected by SSFS [14, 15]. Thus any collision-induced soliton power increase or decrease leads to a corresponding variation in the frequency down-shift rate (and temporal deceleration). In calculating the soliton dynamics in between collisions, we included the full wavelength dependence of the fiber dispersion (see left panel of Fig. 2). It is well established that SSFS is is the main workhorse for generating red-shifted frequency components of the SC spectrum [9,10,16]. Although it may happen that initially MI-generated solitons have pulse-widths that are longer than $7T_m$ (see the right panel of Fig. 2), yet the previously described collision-induced power enhancement of Stokes or "rogue" solitons may lead to significant temporal compression. This means that the expressions used to compute the SSFS should be adapted to describe arbitrary (with respect to T_m) pulse durations. For example, when pulse durations are much shorter than the molecular oscillation period T_m, it is known that the SSFS is merely proportional to pulse energy. In the general case, the SSFS may be described (in soliton units) by the following differential equation for the center frequency ω_0 of any given soliton [14]:

$$\frac{\partial \omega_0}{\partial z} = -\frac{\pi}{8}\int_{-\infty}^{+\infty} d\Omega \Omega^3 \frac{R(\Omega/2\pi t_c)}{sinh^2(\pi\Omega/2)} \tag{8}$$

where $R(\Omega/2\pi t_c)$ is the Raman loss spectrum and t_c is the soliton time width. Differently from [14], we calculated the Raman spectrum R in terms of its standard Lorentzian approximation instead of the linear approximation: however the discrepancy among the two models is only appreciable for solitons durations as short as 10 fs, a range of durations which is beyond the scope of our present study. When applying Eq. (8) in physical units we also consider the variation of dispersion and nonlinear coefficient upon wavelength.

Let us summarize our procedure for describing the evolution of the MI-induced train of solitons along the fiber. By supposing that we exactly know the initial parameters of each soliton (peak power, time duration, carrier frequency, temporal position), then we may separately apply Eq. (8) to describe the free evolution of each soliton frequency and position in-between collisions. As soon as the temporal positions of two solitons coincide, a pair-wise collision takes place so we may apply Eq. (7) for computing their energy exchange, hence updating the soliton peak powers and time durations after the collision. This procedure is repeated for all solitons and for all collisions until the end of the fiber. From the resulting set of soliton trajectories, we focus our attention to the trajectory of the "rogue" soliton, that is that particular soliton which emerges from the fiber with the largest red-shift and peak power.

As the previously described approach requires the knowledge of the input parameters of each soliton, it is necessary to extract this information from the MI-induced break-up of the pump pulse into a soliton train. Indeed this problem has been solved in exact form for the case of a CW pump by Akhmediev since a long time [17, 18]. In the general case of an arbitrary pump pulse profile, the direct integration of the GNLSE may help to estimate the parameters of the generated solitons [19]. In the presence of a noisy pump, different noise realizations can induce fluctuations in the resulting soliton parameters. For the sake of simplicity, we limited ourselves to a simple deterministic but yet relatively accurate analytical estimate of the soliton parameters that results from the MI-induced decay of the pump pulse. Whenever the MI period T_{MI} (we recall that $T_{MI}^2 = 2\pi|\beta_2|/P_P\gamma$) is much shorter than the input pump pulse t_P, we may suppose that the pump pulse is fragmented into a discrete series of time bins of duration T_{MI} each. Each time bin is indexed by k ($k = 0, \pm1, \pm2, ...$, with $k = 0$ for the time bin at the center of the pump pulse). Then we simply suppose that the pump energy within each time bin k is reshaped into a soliton of the same energy. For a gaussian pump pulse profile $P_P \exp(-t^2/\tau_P^2)$, the optical energy in each time bin reads as $E_k = 0.5P_P\tau_P\sqrt{\pi}A_k$, where $A_k = [Erf((2k-1)\varepsilon) - Erf((2(k-1)-1)\varepsilon)]$ and $\varepsilon = T_{MI}/2\tau_P$. The corresponding soliton temporal duration is $\tau_k = 2T_{MI}^2/(\pi^{5/2}\tau_P A_k)$: for relatively long input pump pulses, one simply has $\tau_k = T_{MI}/\pi^2$, i.e. the soliton duration

#159739 - $15.00 USD Received 12 Dec 2011; revised 9 Feb 2012; accepted 27 Feb 2012; published 25 Apr 2012

is independent of the pump duration and is simply proportional to the MI period. Note that, besides the input parameters of the soliton train, it is also necessary to estimate the distance along the fiber where the soliton train is formed from the input pump pulse. Again, for the case of a CW pump, one may obtain such a distance in exact form [17, 18], however in the general case of pump pulses of arbitrary shape and time duration one has to resort to numerical simulations like that of the right panel of Fig. 2 for estimating such a distance.

In the left panel of Fig. 3 we show, for different pump pulse durations, both the number of MI generated solitons as well as the total number of their pair-wise collisions. As it can be seen, the total number of pair-wise collisions grows almost linearly with the number of interacting solitons. From a series of pre-warming simulations with the full GNLSE equations, we have registered the fiber lengths required by the pattern to be formed. We have then integrated our analytical equations over the remaining distance to complete the 8 m of fiber. Whereas the right panel of Fig. 3 provides a qualitative display on how the carrier wavelengths of solitons spread towards longer wavelengths owing to the interplay of SSFS and soliton-soliton collisions. The bunch of solitons is generated by a 10 ps long pump pulse. The analytic integration length was extended to the remaining 4.8*m* since we have estimated from the full solution of the GNLSE that in this case 3.2m are required for the pulse break-up and pattern formation. In the next section, we present a detailed quantitative comparison between the experiments, the full numerical simulations and our simplified analytical model for the soliton train dynamics.

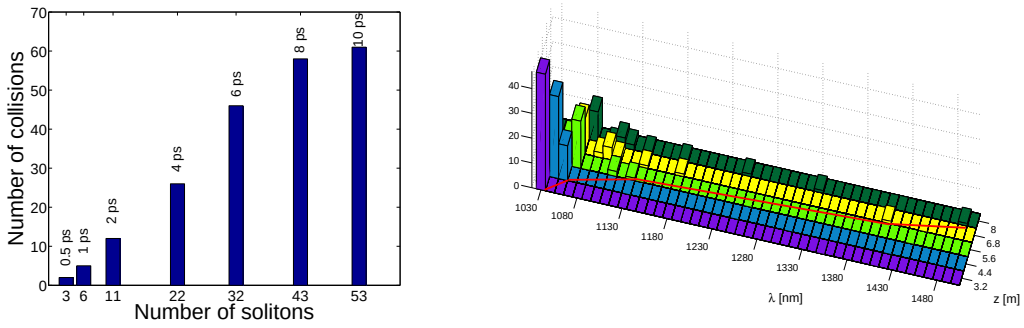

Fig. 3. Left. Number of collisions vs. the total number of solitons in the bunch generated for various pump pulse durations. Right. histogram of the number of solitons upon carrier wavelength for a 10 ps pump pulse, from z=3.2 m to z=8 m. At the origin all the solitons have similar carrier wavelengths, so the histogram has a unique bar.

4. Discussion

In Fig. 4 we show a summary of the comparison among the experimental results on the one side, and both the full GNLSE numerical computations and the predictions of the analytical model for the evolution of the soliton parameters that was derived in the previous section on the other side. In the top frame of the left panel of Fig. 4 we report the analytically computed evolution along the fiber of the central wavelength of the Stokes or ”rogue” soliton with the longest wavelength from the bunch: here the pump pulse duration is equal to 2 ps, which leads to break-up in a soliton train after 1 m. Although a monotonic increase of wavelength with distance of the rogue soliton is observed, Fig. 4 also reveals discontinuities in the slope of such increase which are a result of collisions. Basically each collision boosts the Stokes soliton energy and peak power, so that its SSFS rate is increased after the collision. The bottom frame of the left panel of Fig. 4 illustrates the corresponding evolution with distance of the Stokes soliton

#159739 - $15.00 USD Received 12 Dec 2011; revised 9 Feb 2012; accepted 27 Feb 2012; published 25 Apr 2012

peak power: clearly the power jumps as result of discrete energy increases at collisions. Finally the right panel of Fig. 4 presents an overall picture of the dependence of the long-wavelength edge of the SC spectrum that is obtained from either experiments, simulations and the analytical theory, respectively. In Fig. 4, the blue curve represents the experimental long-wavelength edge of the SC spectral intensity. We evaluate this point by measuring the wavelength where the infrared spectral intensity drops at -10 dB from its flat top value (see the left panel in Fig. 1). As it can be seen, the experiments show that the SC bandwidth increases by more than 200 nm (i.e., from 1200 to about 1430 nm) as the pump pulse duration grows larger from 500 fs up to 10 ps. Fig. 4 shows that the experimental dependence of the spectral enlargement upon pump pulse duration is both qualitatively and quantitatively well captured by the analytical model: here the violet curve indicates the center wavelength of the rogue soliton (as in the top frame of the left panel of the same figure). Indeed, the analytical model predicts that the rogue soliton wavelength grows from 1150 nm (for a 500 fs pump) up to 1490 nm (for a 10 ps pump). Finally, in the right hand panel of Fig. 4, the dots show the predicted long-wavelength edge of the SC from the full numerical solution of the GNLSE (see again the right panel in Fig. 1 for details). Each dot comes from the averaged spectral power (computed at -10dB from the flat top as we did for the experiments). The error-bars show that the difference in noise seeds mainly affects the dynamics of long input pulses. The GNLSE results are in qualitative and quantitative agreement with the experiment.

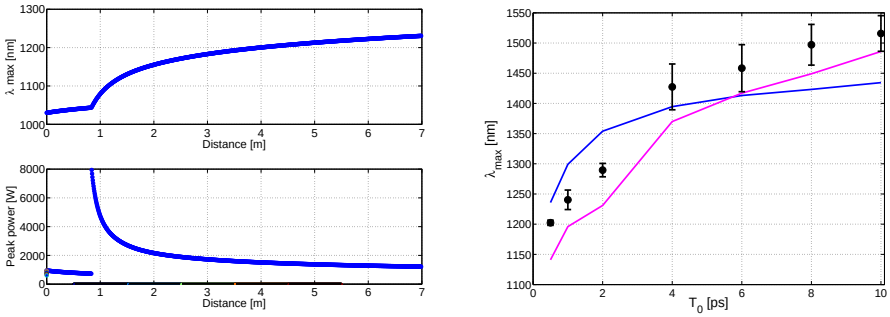

Fig. 4. Left. Analytical prediction of (top frame) the center wavelength or (bottom frame) peak power of the rogue soliton vs distance from pulse break-up (pump pulse of 2 ps); Discontinuities occur at collisions. Right. Pump pulse duration dependence of long-wavelength SC edge. Analytical solution (violet); experimental spectrum (blue curve); numerical GNLSE solution (black dots: average value, error bar: deviation from mean value due to different noise seeds).

5. Conclusion

In our experiments we investigated the dependence of the spectral broadening associated with SC generation in the short-wave infrared from a PCF, by continuously varying the pulse duration of a pump laser centered at 1030 nm. We found out that the infrared spectral broadening is nearly doubled (*i.e.* increased by more than 200 nm) when the pump pulse duration grows from 500 fs up to 10 ps. We have well reproduced the observed continua by full numerical simulations, and elucidated by a simple analytical model that the growth mechanism of the short-infrared spectral components is the Raman-induced energy exchange among colliding solitons. We have presented a detailed analytical description of the SSFS enhancement that is experienced by the most red-shifted soliton, as a result of its energy collection process from all of its neighbors.

#159739 - $15.00 USD Received 12 Dec 2011; revised 9 Feb 2012; accepted 27 Feb 2012; published 25 Apr 2012

Acknowledgment

This work has been carried out in the frame of the European Project NextGenPCF. The authors also acknowledge the partial support from the Université Franco-Italienne under the program VINCI 2010.

#159739 - $15.00 USD Received 12 Dec 2011; revised 9 Feb 2012; accepted 27 Feb 2012; published 25 Apr 2012